Improved Morphological Attributes of Zinc Oxide Nanorods: Effect of Precursor Concentration

Rahma N. Thannoon
Department of Physics/ College of Science/ University of Mosul/ Mosul
Yasir H. Mohammed,
Department of Physics/ College of Education for Pure Science/ University of Mosul/ Mosul
Samir M. Ahmad
Department of Physics/ College of Science/ University of Mosul/ Mosul

corresponding author:
Rahma N. Thannoona
rahma.scp100@student.uomosul.edu.iq

ABSTRACT

This study explored the impact of different concentrations of zinc (Zn) precursor (10, 20, 30, and 40 mM) on the morphological characteristics, element composition, and crystal structure of zinc oxide (ZnO) nanorods (NRs) synthesized on ZnO-seeded glass substrates using a hydrothermal technique. The physical characteristics of ZnO NRs were examined in detail using field emission scanning electron microscope (FESEM), X-ray diffraction (XRD) technique, and energy-dispersive X-ray (EDX) spectroscopy. The results revealed that the grown ZnO NRs strongly depended on the precursor concentrations of the reactants. Using this cost-effective methodology, sundry morphologies of ZnO structures were realized, impacting their morphological, compositional, and structural properties. FESEM results showed that the samples grown using 30 mM concentration had a rods-like structure with vertical alignment and high density, whereas samples grown using $\leq$ 20 mM concentration had a rods-like structure with random alignment and low density. However, the samples synthesized using 40 mM concentration showed marginal growth of the rods. EDX analysis confirmed that O and Zn were the main elements in the synthesized samples, indicating a formation of high-purity ZnO NRs. XRD patterns of the samples shown a polycrystalline wurtzite structure with (002) direction as the prominent peak in all grown samples. In conclusion, this study can enhance the development of ZnO NRs production for various applications.

Keywords: Hydrothermal technique, precursor concentration, ZnO nanorods, seed layer.

INTRODUCTION

ZnO is a semiconductor material that has a significant exciton binding energy of 60 meV at room temperature and a direct wide energy gap (E_g) of 3.37 eV (Xiaming *et al.*, 2009). One-dimensional (1D) ZnO nanostructures (NSs), including NRs, nanowires, nanobelts, and nanotubes, have attracted considerable attention due to their significance in fundamental scientific research and potential applications in electrochemical, electronic, optoelectronic, and electromechanical nano-devices (Yi *et al.*, 2005), as well as bio-sensing (Kim *et al.*, 2014). The high surface area-to-volume ratio and direct carrier conduction path of 1D ZnO NSs confer an advantage over other NSs types (i.e., 0D, 2D, and 3D) (Mustafa *et al.*, 2017). Various methods were employed to synthesize ZnO NRs, such as vapor-liquid-solid (VLS) (Klimovskaya *et al.*, 1996), vapor-solid (VS) (Umar *et al.*, 2007), metal organic chemical vapor deposition (MOCVD) (Kim *et al.*, 2005), chemical bath deposition (CBD) (Willander *et al.*, 2009), and hydrothermal method (Mustafa *et al.*, 2017). Among these methods, the hydrothermal is notable because of its simplicity, cost-effectiveness, energy efficiency in producing ZnO NRs (Jeon *et al.*, 2015), low-temperature growth, vacuum-free, suitable for used different substrates with various shapes and sizes. Moreover, this technique enables the development of ZnO NRs across large surfaces and on various substrates that cannot endure high temperatures (Ateş, 2012). Consequently, this process is a promising method for producing 1D nanomaterials. Numerous studies have demonstrated that several critical parameters, including precursor content (Al-Rasheedi *et al.*, 2022), growth temperature (Mufti *et al.*, 2018), seed-layer type (Akhir *et al.*, 2021), seed-layer thickness (Azmi *et al.*, 2022), doping (Badgujar *et al.*, 2022) and ZnO composites with other substances (Mohammed, 2019), significantly influence the development of ZnO NRs (Abdulrahman *et al.,* 2025). According to reports, the concentration of the precursor has impacted the size and morphology of the formed ZnO NRs (Suhaimi and Yuwono, 2019). This study reports the production of hexagonal-shaped ZnO NRs through a simple hydrothermal method at low temperature and examines the impact of concentration value on the properties of the ZnO NRs. The sample morphologies and structural are characterized utilizing FESEM, XRD, and EDX spectroscopy. The results of the ZnO NRs produced have potential applications as semiconductors in renewable energy devices.

EXPERIMENTAL DETAILS

The samples were prepared through a two-step growth process: (i.e., deposition of a ZnO-seeded layer on a glass substrate using thermal chemical vapor deposition technique (TCVD), followed by the growth of ZnO NRs using hydrothermal method).

Preparation of ZnO as seed layer

ZnO seeded-layer were grown on glass substrate (1×1 cm^2) by TCVD. Zn metal was obtained from high-purity Zn acetate dehydrate (ZnAD) ((CH3COO)$_2$ Zn.2H$_2$O, 99.97%). To get rid of dust and other contaminants, the glass substrates were ultrasonically cleaned in acetone, isopropyl alcohol (IPA), and de-ionized water for eight minutes each. A hot air stream was then used to dry them.

To fabricate a ZnO seeded layer, cleaned glass substrates and an alumina boat containing 1 g of ZnAD powder was arranged on a flat stainless-steel holder, ensuring a consistent separation of 4 cm between the substrates and the boat, within a horizontal double-tube deposition reactor. The heating procedure commenced after the quartz tube was securely sealed with a sealing flange assembly to prevent any leakage into the surrounding environment. The growth temperature was raised to 425°C at a rate of 10°C/min. At the designated evaporation temperature, O$_2$ gas was introduced into the reactor at a flow rate of 200 mL/min. The growth process was maintained for 15 minutes at a pressure of 1 atm (760 Torr). All other growth parameters were carefully regulated throughout the procedure. Once the furnace had naturally cooled to room temperature, the samples were retrieved from the reactor for subsequent analysis.

Preparation of the ZnO NRs

ZnO NRs were grown up by a hydrothermal technique. ZnAD and Hexamethylenetetramine (HMTA, 99.0%, analytical grade, Wako) with different concentrations (10, 20, 30, and 40 mM) were

used as precursors. The precursor solution is prepared in 80 ml of deionized water with pH number of 7, which is adjusted by adding Sodium hydroxide (NaOH) complex solution and stirred about 15 min to guarantee the consistency and dissolution of the materials. A pH-meter (model: Senz pH Duo, manufactured in Malaysia) was utilized to measure the pH values. The mixed solution was carefully transferred into a Teflon autoclave container, where the ZnO-seeded glass substrates were arranged in a horizontal orientation. The hydrothermal autoclave was then subjected to heating in an oven at a temperature of 100 °C for a period of 5 hours. Following this process, the substrate was extracted from the autoclave and subjected to multiple rinses with water to ensure the removal of any residual salt from its surface. Subsequently, it was allowed to dry naturally under ambient conditions.

Characterization techniques

FESEM combined with EDX spectroscopy was used to get surface pictures and verify the growing samples' elemental compositions. Using an X-ray diffractometer (Malvern PANalytical-Aeris) with CuKα ($\lambda = 1.5406$ Å) radiation running at 40 kV and 30 mA, the orientation and crystal structure of the generated samples were confirmed. With an angle step size of 0.011°, the samples were scanned between 25° and 75°.

RESULT AND DISCUSSION

FESEM is among the most effective instruments for examining and analyzing surfaces. Fig. (1: a-d) displays the SEM images of the ZnO NRs formed at different precursor concentrations of Zn of 10, 20, 30, and 40 mM, respectively. For 10 mM Fig. (1a), the samples showed the beginning of the ZnO NRs crystallization process compared with a notable increase in the growth process for the samples grown at higher concentrations of the precursor material Fig. (1b). For concentrations ≤ 20 mM, the samples had a rod-like structure with random alignment and low density. It is evident that at lower concentrations ≤ 20 mM, the supersaturation level of ZnO nuclei remained relatively weak (Suhaimi and Yuwono, 2019), which affected the quality of the grown samples. At 30 mM concentration Fig. (1c), the samples demonstrated clear growth of the ZnO NRs with distinct vertical alignment, hexagonal shape, higher length, and larger density than those prepared at other concentrations. As the concentration increased to 30 mM Fig. (1c), more Zn^{2+} ions were formed, resulting in the growth of ZnO NRs to greater lengths (Amin *et al*., 2011). These findings are consistent with the XRD observations Fig. (2c). In contrast, the samples synthesized using 40 mM concentration Fig. (1d) showed marginal growth of the rods with a decrease in the crystallization process in the direction of the c-axis and a significant decrease in the diameter and length. This is likely due to the precursor reaching a supersaturation level in the solution (Sofyan *et al*., 2019).
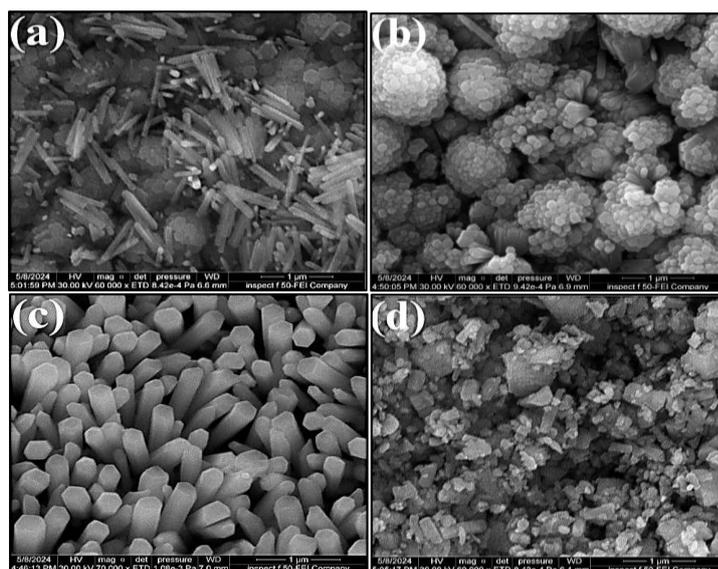

Fig. 1: FESEM images of the ZnO NRs formed using different precursor concentrations of Zn.
(a) 10 mM, (b) 20 mM, (c) 30 mM, and (d) 40 mM.

XRD is a unique analytical methodology used to elucidate the crystalline structure of diverse materials. Fig. (2) shows the characteristic XRD patterns of the ZnO NRs made at various Zn precursor concentrations of 10, 20, 30, and 40 mM, respectively. The diffraction patterns observed across all samples reveal a polycrystalline nature, characterized by a wurtzite structure, with a predominant reflection from the (002) plane at an angle of $2\theta = 34.5°$. Due to the low free surface energy of the (002) plane, ZnO NRs vertically orientated along the (002) direction (Saeed *et al.*, 2024). The XRD peaks noted at 2θ Fig. (2) were matched with the planes (100), (101), (102), (110), (103), and (200) respectively. The crystalline peaks that were noted were in good agreement with the regular peaks indicated in the JCPDS card. No. 36-1451 and 96-101-1259 card. Several researchers (Abdulrahman *et al.*, 2021; Wahab *et al.*, 2009) also noticed similar kinds of crystalline peaks for ZnO NRs. The intense and acute diffraction of (002) peaks Fig. (2) verify the prepared samples' high degree of crystallization (Ahmad and Mohammed, 2023). Improved crystal quality was achieved as more Zn and O ions move to the proper growth sites (Mustafa *et al.*, 2017). Changing the precursor concentrations of Zn, impact on ZnO NRs' crystal quality. The synthesized ZnO NRs have been orientated in various directions, as evidenced by the high intensity peaks (002), (100), and (101) (Suryanarayana *et al.*, 1998). Equations (1 and 4) (Murty *et al.*, 2013) were used to calculate the structural parameters of ZnO NRs samples from the XRD patterns. The results were shown in (Table 1) and included average crystallite size (D), lattice strain (ε), dislocation density (δ), and the interplanar distance (spacing) (d):

$$D = (0.94\,\lambda\,)/(\beta\,cos\,\theta\,) \quad \dots\dots\dots (1)$$
$$\varepsilon = \beta/4tan\theta \quad \dots\dots\dots (2)$$
$$\delta = 1/D^\wedge 2 \quad \dots\dots\dots (3)$$
$$d(hkl) = \lambda/2sin\theta \quad \dots\dots\dots (4)$$

Where λ is the wavelength of the X-ray radiation source, β is the full width at half-maximum (FWHM) of the diffraction peak in radians, θ is the Bragg angle of the diffraction peak, and hkl are the Miller indices of the plane of crystal. As illustrated in Fig. (2), The (002) plane's peak intensity was enhanced by the increase of precursor concentrations. The D and ε influence the shift in Bragg peak position, FWHM, and intensity (Abbas *et al.*, 2016). Therefore, the observed variation in the (002) plane intensities for ZnO NRs, as depicted in Fig. (2), can be attributed to changes in crystallite size and lattice strain effects.

Table 1: XRD result and structural parameters of the ZnO NRs formed using different precursor concentrations of Zn.

Zn precursor concentration (mM)	hkl	2Θ (deg.)	FWHM (deg.)	d (nm)		D (nm)	$\delta*10^{-3}$ (nm)$^{-2}$	ε
				Standard	Calculated			
10	002	34.4	0.2984	0.26	0.260	29.1	1.18	0.004206
20	002	34.3	0.1292	0.26	0.261	67.2	0.22	0.001827
30	002	34.5	0.2838	0.26	0.259	30.6	1.07	0.003988
40	002	34.5	0.2087	0.26	0.259	41.6	0.58	0.002933

The EDX characteristics have been applied for various Zn precursor concentration values, to study the elemental chemical composition and their distribution. Fig. (3) display the existence of the Zn and O elements with substrate elements signal (Ca and Si). The minor peaks present in the spectrum, such as C is attributed to the carbon material pre-coating applied to prevent sample charging during FESEM characterization (Ghazali *et al.*, 2021). EDX analysis confirmed that O and Zn were the main elements in the synthesized samples, indicating a formation of high-purity ZnO NRs (Ahmad and Mohammed, 2023). (Table 2) give the atomic and weight percentage of each element of the ZnO NRs formed using different precursor concentrations of Zn.

Table 2: EDX result of elemental chemical composition of the ZnO NRs formed using different precursor concentrations of Zn.

Zn conc. (mM)	Atomic %					Weight %				
	C	Ca	Si	O	Zn	C	Ca	Si	O	Zn
10	41.6	0.5	1.3	24.7	32.0	16.4	0.7	1.2	13.0	68.7
20	26.2	0.2	0.0	39.6	34.0	10.3	0.3	0.0	19.9	69.5
30	26.2	0.2	0.4	39.5	33.7	9.4	0.3	0.4	20.1	69.8
40	25.6	0.0	0.0	35.7	38.6	9.0	0.0	0.0	16.8	74.2
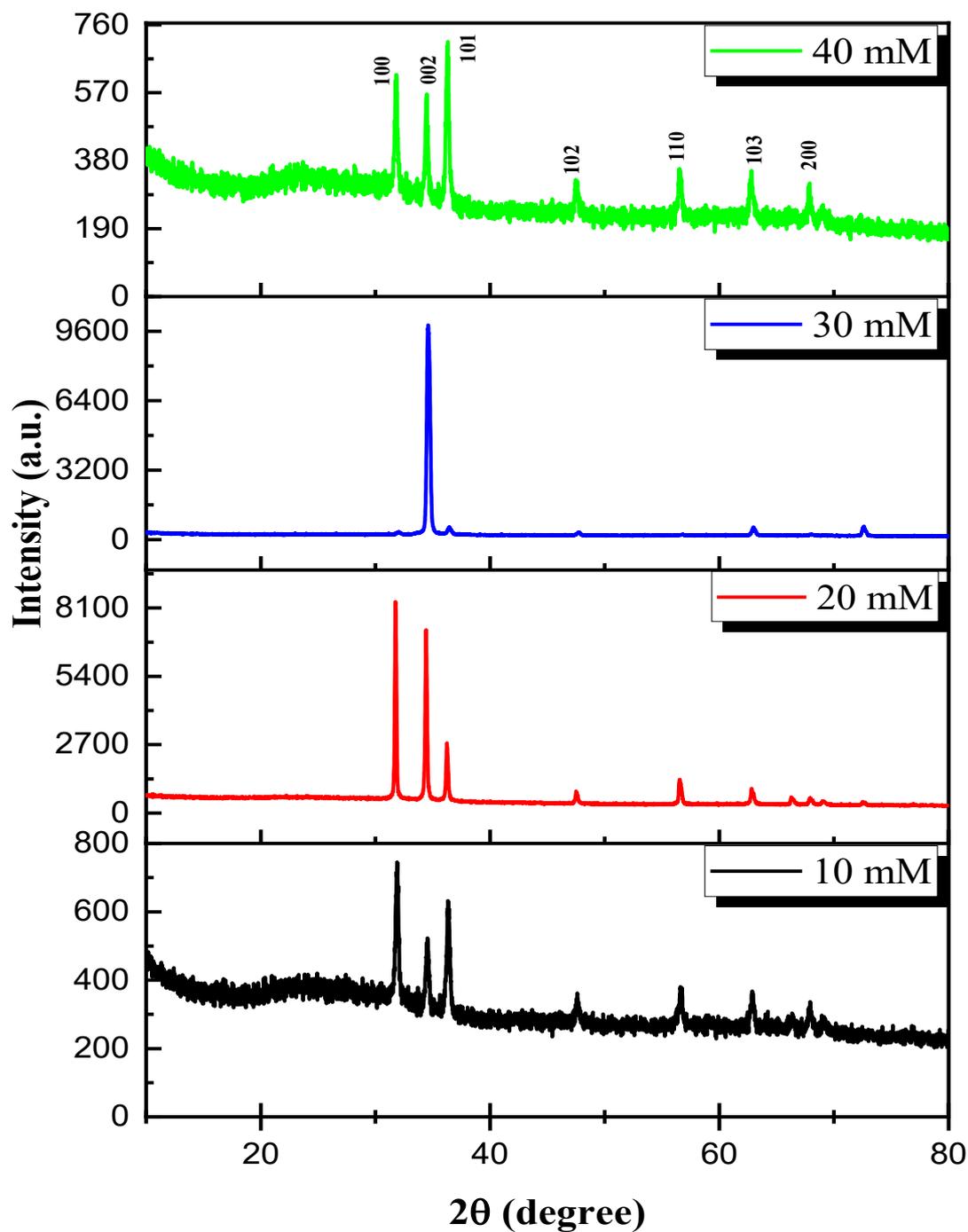
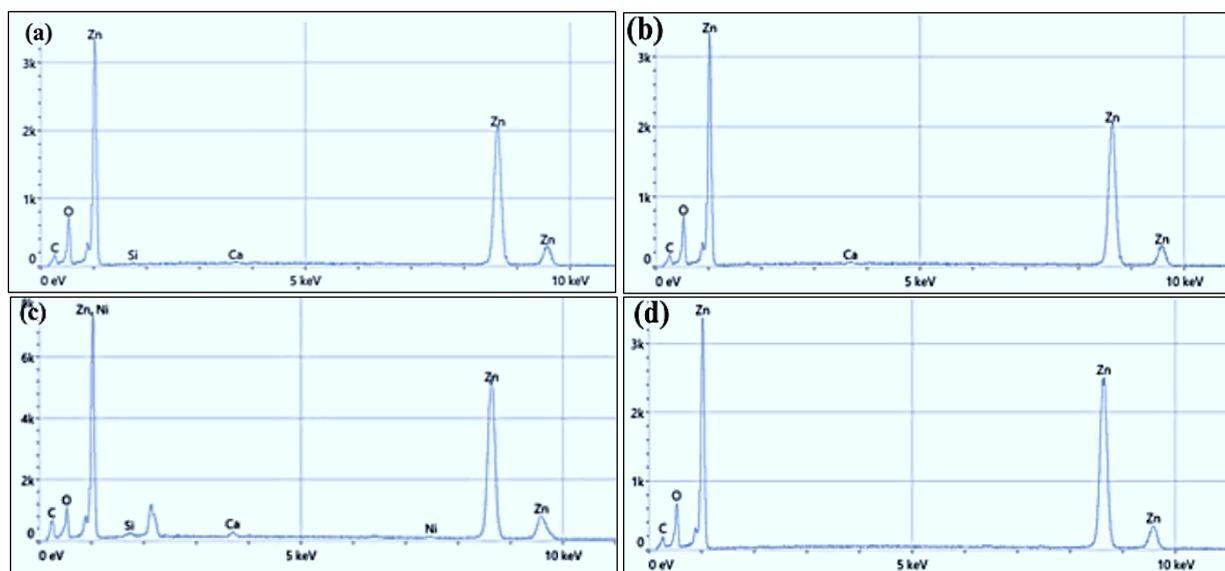**Fig. 2: X-ray diffraction of the ZnO NRs formed using different precursor concentrations of Zn.**

Fig. 3: The EDX characteristics of the ZnO NRs formed using different precursor concentrations of Zn (a) 10 mM, (b) 20 mM, (c) 30 mM, and (d) 40 mM.

CONCLUSIONS

In conclusion, well-aligned ZnO NRs were synthesized on ZnO-seeded glass substrates via a hydrothermal method, utilizing different precursor concentrations of Zn (10, 20, 30, and 40 mM). The morphological analysis indicates that precursor concentration is an acute factor influencing the surface morphology and crystalline structure of the synthesized samples. FESEM images demonstrated that the growth of ZnO NRs is greatly dependent on the precursor concentrations of Zn, with the optimal ZnO NRs achieved at a concentration of 30 mM. This finding is corroborated XRD analysis, which reveals a polycrystalline nature characterized by a wurtzite structure, vertically aligned along the (002) plane at the c-axis, with an average crystal size (D) of approximately 31 nm. EDX analysis confirmed that oxygen and zinc were the predominant elements in the prepared samples, indicating the formation of high-purity ZnO NRs. Consequently, this study may enhance the development of ZnO NRs production for various applications.

REFERENCES

Abbas, K.N.; Bidin, N.; Sabry, R.S.; Al-Asedy, H.J.; Al-Azawi, M.A.; Islam, S. (2016). Structures and emission features of high-density ZnO micro/nanostructure grown by an easy hydrothermal method. *Mat. Chem. Phy.*, **182**, 298-307. DOI:10.1016/j.matchemphys.2016.07.035

Abdulrahman, A.F.; Ahmed, S.M.; Hamad, S.M.; Almessiere, M.A.; Ahmed, N.M.; Sajadi, S.M. (2021). Effect of different pH values on growth solutions for the ZnO nanostructures. *Chinese J. Phy.*, **71**, 175-189. DOI:10.1016/j.cjph.2021.02.013

Abdulrahman, A.F.; Mostafa, S.H.; Ahmed, S.M.; Abdulqodus, A.N.; Kareem, A.A.; Ahmed, S.M.; Abdulqodus, A.N.; Kareem, A.A.; Ahmed, S.M.; Azizf, S.B.; Almessiere, M.A.; Hamadj, S.M.; Shaikhah, D. (2025). Influence of annealing temperature of seed layer on the structural and optical properties of ZnO nanorods synthesized by SILAR and CBD techniques. *Mat. Tech.*, **40**(1), 2443205. DOI:10.1080/10667857.2024.2443205

Ahmad, I.A.; Mohammed, Y.H. (2023). Synthesis of ZnO nanowires by thermal chemical vapor deposition technique: Role of oxygen flow rate. *Micro Nanostr.*, **181**, 207628. DOI:10.1016/j.micrna.2023.207628

Akhir, R.; Umbaidilah, S.; Abdullah, N.; Buniyamin, I.; Rusop, M.; Khusaimi, Z. (2021). Comparative study on morphology, structural and optical properties of non-seeded and seeded ZnO nanorods. Paper presented at the recent trends in manufacturing and materials towards industry 4.0: Selected articles from iM3F 2020, Malaysia. DOI:10.1007/978-981-15-9505-9_84

Al-Rasheedi, A.; Alonizan, N.; Ansari, A.R.; Abdel-Daiem, A.; Aida, M. (2022). Influence of salt solution concentration on structural properties of ZnO nanorods grown by hydrothermal method. *App. Phy. A*, **128**(9), 782. DOI:10.1007/s00339-022-05937-8

Amin, G.; Asif, M.; Zainelabdin, A.; Zaman, S.; Nur, O.; Willander, M. (2011). Influence of pH, precursor concentration, growth time, and temperature on the morphology of ZnO nanostructures grown by the hydrothermal method. *J. Nan.*, **2011**(1), 269692. DOI:10.1155/2011/269692

Ateş, E.S. (2012). Hydrothermally grown zinc oxide nanowires and their utilization in light emitting diodes and photodetectors. Middle East Technical University (Turkey). A thesis submitted to the graduate school of natural and applied sciences of middle east technical university

Azmi, Z.H.; Mohd Aris, S.N.; Abubakar, S.; Sagadevan, S.; Siburian, R.; Paiman, S. (2022). Effect of seed layer on the growth of zinc oxide nanowires by chemical bath deposition method. *Coat.*, **12**(4), 474. DOI:10.3390/coatings12040474

Badgujar, A.C.; Yadav, B.S.; Jha, G.K.; Dhage, S.R. (2022). Room temperature sputtered aluminum-doped ZnO thin film transparent electrode for application in solar cells and for low-band-gap optoelectronic devices. *ACS Ome.*, **7**(16), 14203-14210. DOI:10.1021/acsomega.2c00830

Ghazali, M.N.I.; Izmi, M.A.; Mustaffa, S.N.A.; Abubakar, S.; Husham, M.; Sagadevan, S.; Paiman, S. (2021). A comparative approach on one-dimensional ZnO nanowires for morphological and structural properties. *J. Cry. Grow.*, **558**, 125997. DOI:10.1016/j.jcrysgro.2020.125997

Jeon, E.H.; Yang, S.; Kim, Y.; Kim, N.; Shin, H.-J.; Baik, J.; Kim, H.S.; Lee, H. (2015). Comparative study of photocatalytic activities of hydrothermally grown ZnO nanorod on Si (001) wafer and FTO glass substrates. *Nano. Res. Lett.*, **10**, 1-8. DOI:10.1186/s11671-015-1063-4

Kim, J.Y.; Jo, S.-Y.; Sun, G.-J.; Katoch, A.; Choi, S.-W.; Kim, S.S. (2014). Tailoring the surface area of ZnO nanorods for improved performance in glucose sensors. *Sen. Actu. B: Chem.*, **192**, 216-220. DOI:10.1016/j.snb.2013.10.113

Kim, S.-W.; Fujita, S.; Fujita, S. (2005). ZnO nanowires with high aspect ratios grown by metalorganic chemical vapor deposition using gold nanoparticles. *App. Phy. Lett.*, **86**(15). DOI:10.1063/1.1883320

Klimovskaya, A.; Ostrovskii, I.; Ostrovskaya, A. (1996). Influence of growth conditions on morphology, composition, and electrical properties of n-Si wires. *Phy. Stat. S. (a)*, **153**(2), 465-472. DOI:10.1002/pssa.2211530221

Mohammed, Y.H. (2019). Fabrication of n-MgZnO/p-Si heterojunction diode: Role of magnesium doping. *Super. Microstr.*, **131**, 104-116. DOI:10.1016/j.spmi.2019.06.001

Mufti, N.; Laila, I.K.; Idiawati, R.; Fuad, A.; Hidayat, A.; Taufiq, A. (2018). The effect of growth temperature on the characteristics of ZnO nanorods and its optical properties. *J. Phys.*, Conference Series. DOI:10.1088/1742-6596/1057/1/012005

Murty, B.S.; Shankar, P.; Raj, B.; Rath, B.B. Murday, J. (2013). "Textbook of Nanoscience and Nanotechnology". Springer, Universities press. DOI:10.1007/978-3-642-28030-6

Mustafa, M.; Iqbal, Y.; Majeed, U.; Sahdan, M. (2017). Effect of precursor's concentration on structure and morphology of ZnO nanorods synthesized through hydrothermal method on gold surface. *J. Appl. Phy.* **98**, 041301. DOI:10.1063/1.1992666

Saeed, Z.M.; Mohammed, Y.H.; Ahmad, S.M. (2024). Atmospheric pressure chemical vapor deposition grown one-dimensional ZnO nanostructures. *Phy. Sol. Sta.*, **66**(7), 201-213. DOI:10.1134/S1063783424600742

Sofyan, N.; Panjaitan, S.P.; Yuwono, A.H. (2019). Growth of ZnO nanorods synthesized via chemical bath deposition at different reaction times and precursor concentrations. *Mat. Sci. Eng.* **553**, 012056. DOI:10.1088/1757-899X/553/1/012056

Suhaimi, L.; Yuwono, A. (2019). Optical properties of ZnO nanorods derived from chemical bath deposition process with different seeds solution concentration. *Mat. Sci. Eng.*, **541**, 012034. DOI:10.1088/1757-899X/541/1/012034

Suryanarayana, C.; Norton, M.G.; Suryanarayana, C.; Norton, M.G. (1998). "X-rays and Diffraction". Springer US, pp. 3-19. DOI:10.1007/978-1-4899-0148-4_1

Umar, A.; Kim, S.; Kim, J.; Park, Y.; Hahn, Y.B. (2007). Structural and optical properties of single-crystalline ultraviolet-emitting needle-shaped ZnO nanowires. *Mat. Lett.*, **61**(27), 4954-4958. DOI:10.1016/j.matlet.2007.03.079

Wahab, R.; Kim, Y.-S.; Shin, H.-S. (2009). Synthesis, characterization and effect of pH variation on zinc oxide nanostructures. *Mat. Trans.*, **50**(8), 2092-2097. DOI:10.2320/matertrans.M2009099

Willander, M.; Nur, O.; Zhao, Q.; Yang, L.; Lorenz, M.; Cao, B.; Pérez, J.Z.; Czekalla, C.; Zimmermann, G.; Grundmann, M.; Bakin, A.; Behrends, A.; Al-Suleiman, M.; El-Shaer, A.; Mofor, A.C.; Postels, B.; Waag, A.; Boukos, N.; Travlos, A.; Kwack, H.S.; Guinard J.; Grundmann, M. (2009). Zinc oxide nanorod based photonic devices: recent progress in growth, light emitting diodesand lasers. *Nanotech.*, **20**(33), 332001. DOI:10.1088/0957-4484/20/33/332001

Xiaming, Z.; Huizhen, W.; Shuangjiang, W.; Yingying, Z.; Chunfeng, C.; Jianxiao, S.; Zijian, U.; Xiaoyang, D.; Shurong, D. (2009). Optical and electrical properties of N-doped ZnO and fabrication of thin-film transistors. *J. Semicon.*, **30**(3), 033001. DOI:10.1088/1674-4926/30/3/033001

Yi, G.-C.; Wang, C.; Park, W. I. (2005). ZnO nanorods: Synthesis, characterization and applications. *Semicon. Sci. Tech.*, **20**(4), S22. DOI:10.1088/0268-1242/20/4/003

تحسين الصفات المورفولوجية لقضبان أوكسيد الخارصين النانوية: تأثير تركيز السلائف

رحمة نذير ذنون

قسم الفيزياء/ كلية العلوم/ جامعة الموصل/ الموصل

ياسر حسين محمد

قسم الفيزياء/ كلية التربية للعلوم الصرفة/ جامعة الموصل/ الموصل

سمير محمود أحمد

قسم الفيزياء/ كلية العلوم/ جامعة الموصل/ الموصل

الملخص

استكشفت هذه الدراسة تأثير تركيزات مختلفة من سلائف الخارصين (10, 20, 30, and 40 mM) على الخصائص المورفولوجية وتركيب العناصر والبنية البلورية لقضبان أوكسيد الخارصين النانوية (ZnO NRs) المصنعة على ارضيات زجاجية بطبقة محفزة من أوكسيد الخارصين (ZnO) باستخدام تقنية التوليف الحراري المائي. تم فحص الخصائص الفيزيائية لـ ZnO NRs بالتفصيل باستخدام المجهر الإلكتروني الماسح بالانبعاث الميداني (FESEM) وطيف الأشعة السينية المشتتة للطاقة (EDX) وتقنية حيود الأشعة السينية (XRD). كشفت النتائج أن لـ ZnO NRs المحضرة تعتمد بشدة على تركيز سلائف المواد المتفاعلة. باستخدام هذه المنهجية الفعالة من حيث التكلفة، تم تحقيق أشكال مختلفة من هياكل ZnO ، مما أثر على خصائصها المورفولوجية والتركيبية والبنيوية. أظهرت نتائج FESEM أن العينات المحضرة باستخدام تركيز 30 mM لها بنية تشبه القضبان ذات محاذاة رأسية وكثافة عالية، في حين أن العينات المحضرة باستخدام تركيز 20 mM ≤ لها بنية تشبه القضبان ذات محاذاة عشوائية وكثافة منخفضة. ومع ذلك، أظهرت العينات المحضرة باستخدام تركيز 40 mM نموا هامشيا للقضبان. أكد تحليل EDX أن Zn و O هما العنصران الرئيسيان في العينات المصنعة، مما يشير إلى تكوين ZnO NRs عالية النقاء. كشفت أنماط XRD للعينات عن بنية سداسية wurtzite متعددة التبلور مع اتجاه (002) باعتباره الذروة السائدة في جميع العينات المحضرة. بالنتيجة، يمكن لهذه الدراسة أن تعزز تطوير إنتاج ZnO NRs لتطبيقات مختلفة.

الكلمات الدالة: تقنية التوليف الحراري المائي، تركيز السلائف، قضبان نانوية من ZnO، طبقة محفزة.